COBEM 2023 27TH INTERNATIONAL CONGRESS OF MECHANICAL ENGINEERING

ABCM Brazilian Society of Mechanical Sciences and Engineering
27th ABCM International Congress of Mechanical Engineering
December 04-08, 2023, Florianópolis-SC, Brazil

COB-2023-2434
DEVELOPMENT OF A TRACTION CONTROL STRATEGY AND DYNAMIC MODELING OF A 4WD ELECTRIC TRACTOR
27th COBEM

Weslen Lins de Araujo
Tárcio André Dos Santos Barros
Vinícius de Galiza Vieira
Faculty of Mechanical Engineering of the State University of Campinas - UNICAMP, Mendeleyev St., 200, Barão Geraldo Campinas - SP
w203979@dac.unicamp.br, tarcio87@unicamp.br, v245284@dac.unicamp.br

Gabriel Del Alamo Cardoso De Moraes
Ivan Camilo Arbelaez Ruiz
Jenyffer Da Silva Gomes Santos
Angel Pontin Garcia
Daniel Albiero
Agricultural Engineering College, State University of Campinas - UNICAMP.

Abstract. *The electrification of agricultural tractors offers greater versatility in the development of embedded controls. Electric tractors equipped with independent motors on each wheel have the ability to individually control torque and speed, adapting to the traction capacity of each wheel, which is affected by disturbances along the path, resulting in a decrease in operational efficiency. To achieve this goal, it is essential to carry out a thorough mathematical modeling of the entire system, which will serve as the basis for the development of these controls. This article proposes a dynamic modeling of an electric tractor and a traction control strategy, with the aim of being used in the development of future embedded systems, aiming to enhance the operational efficiency of an electric tractor. Tire-soil interaction and electrical motor mathematical models were used for simulation in Matlab Simulink® software, reproducing the operation of an agricultural tractor with a drag implement. Disturbances were introduced into the system, such as variations in the ground slope angle and the action of the drag implement. For the traction control strategy, a method of torque distribution between the front and rear axles was proposed, generating a power distribution map, showing percentage values of action on each axle to achieve maximum traction efficiency. The simulation results demonstrated the expected behavior in the presence of disturbances, such as an increase in front-wheel slip with the ground slope, reaching over 70% growth at a 10º incline, highlighting the importance of modeling for estimating these traction parameters for the development of future traction control systems to enhance operational efficiency*.

Keywords: *traction control, tire-soil interaction, wheel slip*

1. INTRODUCTION

Conventional vehicles with internal combustion engines feature a gearbox divided into gears to provide different torque ranges based on power and velocity demands. The torque distribution between front and rear wheels in the case of four-wheel drive (4WD) is governed by a constant relationship determined by the drive shafts gear ratio. The use of individual electric motors to drive each wheel individually allows for selective torque distribution to each wheel as needed. This characteristic of electric vehicles with individual motors expands the possibilities for developing control systems with various objectives, such as speed control, drivability for autonomous vehicles, and torque optimizers for maximum traction efficiency, as demonstrated by some authors such as Chen et al. (2019), J. Wang et al. (2021), and Cong et al. (2018).

Tractors that utilize electric motors as their source of propulsion possess a wide range of speed regulation and high operational efficiency. However, research for the development of control systems is insufficient given the complexity of their operation (Xie et al., 2022). The enhancement of mathematical models of these tractors' dynamics has been conducted to introduce new embedded control systems, as demonstrated by S. Wang et al. (2023), who developed a control strategy for electric tractors with two motors to achieve high operational efficiency under various conditions. The authors modeled power transfer within the vehicle and its gear shifting. The system proposed combines on-demand torque calculation and driving torque distribution based on nonlinear PID control, and a modified Snake-type optimization algorithm, resulting in significant improvements in tractor efficiency and stability, particularly during plowing. Osinenko and Streif (2017) developed a traction control system to optimize the energy efficiency of the electric tractor RigiTrac

EWD 120 by estimating the soil resistance coefficient using a Kalman filter. These control systems undergo a conceptualization and testing process in computational environments before being implemented in real-world situations. Therefore, it is advantageous to create an accurate simulation of the dynamics of a tractor, considering its interaction with the ground and various operating scenarios. The dynamics of agricultural tractor operations involving drag implements such as seeders and plows require constant speeds, implying an increase or decrease in torque at each wheel based on various field scenarios that involve changes in speed, slope angle, soil type, and input consumption. The aim of this work was to develop a dynamic model of an electric tractor equipped with a drag implement, taking into account different operating conditions and off-road tire-soil interaction, using Matlab Simulink® software. Additionally, a traction control strategy was created through optimal power distribution maps for the wheels, aiming the maximum traction efficiency.

2. METHODOLOGY

2.1 Longitudinal dynamic of electric tractor

A longitudinal vehicle model, as depicted in Figure 1, was utilized to obtain the motion equations for a 4WD electric tractor, using the sum of forces described in Eq. (1) and the sum of moments in Eq. (2).

$$\boldsymbol{2GT_f}(t) - \boldsymbol{MR_f}(t) + \boldsymbol{2GT_r}(t) - \boldsymbol{MR_r}(t) - (\boldsymbol{W} + \boldsymbol{m}(t)\boldsymbol{g})\,\boldsymbol{sin}\,\boldsymbol{\alpha}(t) - \boldsymbol{P}(t)\,\boldsymbol{cos}\,\boldsymbol{\theta}\,(t) = (\boldsymbol{W} + \boldsymbol{m}(t)\boldsymbol{g})\ddot{\boldsymbol{x}}, \quad (1)$$

$$\boldsymbol{I}\dot{\boldsymbol{\omega}}_{\boldsymbol{i}}(t) = \boldsymbol{T_i}(t) - \boldsymbol{r_i}(t)\boldsymbol{GT_i}(t), \quad (2)$$

where $\boldsymbol{GT_i}$, $\boldsymbol{MR_i}$, $\boldsymbol{W}$, $\boldsymbol{m}$, $\boldsymbol{\alpha}$, $\boldsymbol{\theta}$, $\boldsymbol{P}$, $\boldsymbol{g}$, and $\ddot{\boldsymbol{x}}$ represent the gross traction force, rolling resistance, tractor weight, mass of planting inputs, ground slope angle, angle of inclination of the implement draft, force of the implement, acceleration due to gravity, and vehicle acceleration, respectively. $\boldsymbol{I}$, $\dot{\boldsymbol{\omega}}_{\boldsymbol{i}}$, $\boldsymbol{T_i}$ and $\boldsymbol{r_i}$ denote the momentum of inertia of the wheel, angular velocity of the wheel, torque produced at the wheel, and dynamic wheel radius, respectively. The dynamic wheel loads for each wheel are calculated through the sum of forces and moments, as suggested by Rajamani (2012) and Macmillan (2010), using dimensional parameters. These parameters include $\boldsymbol{x_f}$, $\boldsymbol{x_r}$, $\boldsymbol{x}$, $\boldsymbol{x'}$, $\boldsymbol{y_g}$ and $\boldsymbol{y_p}$, which represent the distance from the center of mass to the front wheel, rear wheel, wheelbase, distance from the rear wheel to the implement draft, height of the center of gravity, and height of the implement hitch, respectively.

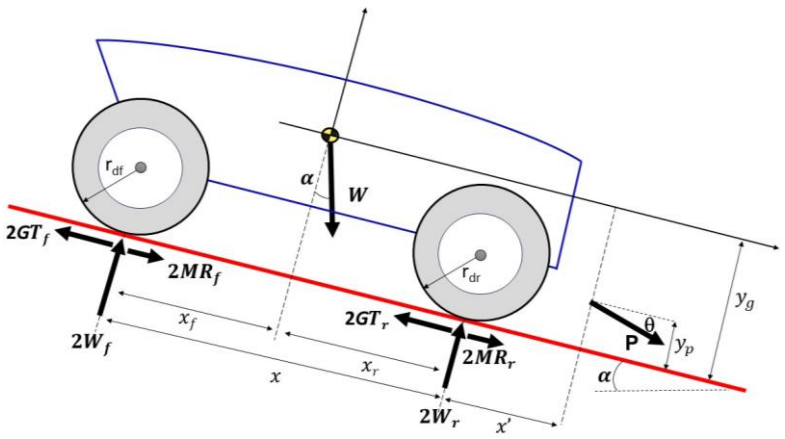

Figure 1. Longitudinal forces acting on a tractor moving on an inclined road.

2.2 Soil-wheel interaction model

The soil-tire interaction model used was developed by Brixius (1987), involving traction parameters such as soil properties, tire dimensions, slip, and dynamic weight. The gross traction force, $\boldsymbol{GT_i}$, and rolling resistance, $\boldsymbol{MR_i}$, are depicted in Eq. (3) and Eq. (4), respectively.

$$\boldsymbol{GT_i}(t) = \boldsymbol{W_i}\left(\mathbf{0.88}\left(\mathbf{1} - \boldsymbol{e}^{-\mathbf{0.1}\boldsymbol{B_n}(t)}\right)\left(\mathbf{1} - \boldsymbol{e}^{-\mathbf{7.5}\boldsymbol{s}(t)}\right) + \mathbf{0.04}\right), \quad (3)$$

$$\boldsymbol{MR_i}(t) = \boldsymbol{W_i}\left(\frac{\mathbf{1.0}}{\boldsymbol{B_n}(t)} + \mathbf{0.04} + \frac{\mathbf{0.5}\boldsymbol{s}(t)}{\sqrt{\boldsymbol{B_n}(t)}}\right), \quad (4)$$

where $\boldsymbol{W_i}$, $\boldsymbol{B_n}$, and $\boldsymbol{s}$, represents the dynamic weight, mobility number, and slip of wheel $\boldsymbol{i}$ respectively.

The Mobility number $\boldsymbol{B_n}$ is given by Eq. 5, as demonstrated by Grisso et al. (2006). This coefficient carries information about tire and soil paraments, such as tire dimensions and soil penetration resistance.

$$\boldsymbol{Bn} = \left(\frac{\boldsymbol{CIbd}}{\boldsymbol{W}}\right)\left(\frac{\boldsymbol{1+5\left(\frac{\delta}{h}\right)}}{\boldsymbol{1+3\left(\frac{b}{d}\right)}}\right), \tag{5}$$

where $\boldsymbol{CI}$, $\boldsymbol{b}$, $\boldsymbol{d}$, $\boldsymbol{\delta}$ and $\boldsymbol{h}$ are the cone index, unloaded tire section width, unloaded tire diameter, tire deflection and tire section height, respectively.

The slip of each wheel is determined by Eq. 6,

$$\boldsymbol{s} = \boldsymbol{1} - \frac{\boldsymbol{v_a}}{\boldsymbol{v_t}}, \tag{6}$$

where $\boldsymbol{v_a}$ and $\boldsymbol{v_t}$ represent the actual tractor forward velocity and the wheel's tangential velocity, respectively.

2.3 Motor drive system

Considering the quick response of the electric motor in comparison to the rest of the system, a simplification of its dynamics was performed to a first-order model, as shown in Eq. (7). The critical aspect of the model response is the critical torque values as a function of the actual motor rotation. For these critical values, a torque map has been implemented in relation to rotation, using data supplied by the manufacturer, in order to manage these torque limits.

$$\boldsymbol{T} = \frac{\boldsymbol{T_d}}{\boldsymbol{\tau s+1}}, \tag{7}$$

where $\boldsymbol{T}$, $\boldsymbol{T_d}$, and $\boldsymbol{\tau}$ represent the torque produced by the electric motor, torque demand, and the time-delay constant of the electric motor, respectively.

2.4 Operation modelling

The operation of tractors with drag implements, such as seeders, can be divided into two phases: maneuvering operation and working operation. During the maneuvering operation, the tractor moves freely with the implement raised, exerting negligible drag force, and without consuming inputs (seeds and fertilizer). In the working operation, the implement penetrates the soil, requiring great drag force, initiating the consumption of inputs, and consequently, reducing the dynamic weight.

2.5 Power distribution

In order to achieve maximum traction efficiency through the manipulation of electric motor torque as a control variable, a power distribution model based on the tractor's power demand, $\boldsymbol{P_d}$, as shown in Eq. 8, is proposed. The demand force $\boldsymbol{F_d}$ can be distributed between the front axle $\boldsymbol{F_{df}}$ and the rear axle $\boldsymbol{F_{dr}}$, aiming to prioritize the axle with greater traction capacity, according to the dynamic weight distribution, which is influenced by variations in the terrain profile and soil properties.

$$\boldsymbol{P_d} = \boldsymbol{v_a}\left(\left(\boldsymbol{W} + \boldsymbol{g}\,\boldsymbol{m}(t)\right)\boldsymbol{sin}\,\boldsymbol{\alpha}(\boldsymbol{t})\right), \tag{8}$$

The distribution of force demand and, consequently, power is determined by the distribution constant $\boldsymbol{a}$ which varies between 0 and 1, where an optimal value needs to be found by the controller to achieve the user's objective. In other words, each motor will independently produce a torque value according to the traction parameters of each wheel. Equation 9 shows the equation for the distribution of demand force, where the force on the front and rear wheels is presented in Equations 10 and 11.

$$\boldsymbol{F_d} = \boldsymbol{F_{df}} + \boldsymbol{F_{dr}}, \tag{9}$$

$$\boldsymbol{F_{df}} = \boldsymbol{F_d a}, \tag{10}$$

$$\boldsymbol{F_{dr}} = \boldsymbol{F_d}(\boldsymbol{1} - \boldsymbol{a}), \tag{11}$$

The traction force of each wheel is equivalent to the net traction produced by the torque applied by the electric motor and the power loss generated by rolling resistance. With the optimal value of $\boldsymbol{\alpha}$ known, the electric motor will provide torque to achieve the ideal front and rear distribution.

2.6 Implementation of the models in a computational environment

The models were implemented in Matlab Simulink®, and various operational scenarios and soil conditions were simulated. The operation cycle was divided into three stages. In the first stage, the tractor starts from rest using a torque ramp function, reaching 150 Nm equally on each wheel, with the aim of maintaining an equal power distribution on all wheels and preserving the tractor's dynamics without external control interference. After 10 seconds, the working operation begins, during which the implement penetrates the soil and consumes the planting inputs. Then, after 45 seconds, the vehicle enters the maneuvering mode, and the cycle repeats when the time reaches 65 seconds. These simulations are performed on tilled soil with a cone index of 900 kPa. A random function was used to simulate the effect of small variations in this soil index, since this variability has a significant influence on the dynamics of the entire system. The ground slope angle $\boldsymbol{\alpha}$ varies along the path of the vehicle: starting at zero, increasing to 10º between distances of 50 and 150 meters, and then returning to zero. Figure 2 illustrates the system dynamics framework with the input parameters, such as the angles $\boldsymbol{\alpha}(t)$, $\boldsymbol{\theta}(t)$, and the soil type through $\boldsymbol{Bn}(t)$. The vehicle and soil parameters are shown in Table 1.

Table 1. Parameters of the vehicle and soil.

Parameter	**Value**
W - Vehicle weight (N)	13000
P - Implement draft (N)	6000
m - Mass of planting inputs (kg)	600
τ - Time-delay constant of motor	1
b - Unloaded tire section width (m)	0.22
d - Unloaded tire diameter (m)	0.51
r - Tire rolling radius (m)	0.26
δ - Tire deflection (m)	0.05
h - Tire section height (m)	0.21
I - Moment of inertia of the wheel (kg.m^2)	6.08
x_f - Distance from the center of mass to the front wheel (m)	1.50
x_r - Distance from the center of mass to the rear wheel (m)	1.50
x - Wheelbase (m)	3
x' - Distance from the rear wheel to the implement draft (m)	1
y_g - Height of the center of gravity (m)	1.50
y_p - Height of the implement draft (m)	0.82
θ - Angle of inclination of the implement draft (rad)	0.17
CI - Cone index (kPa)	900

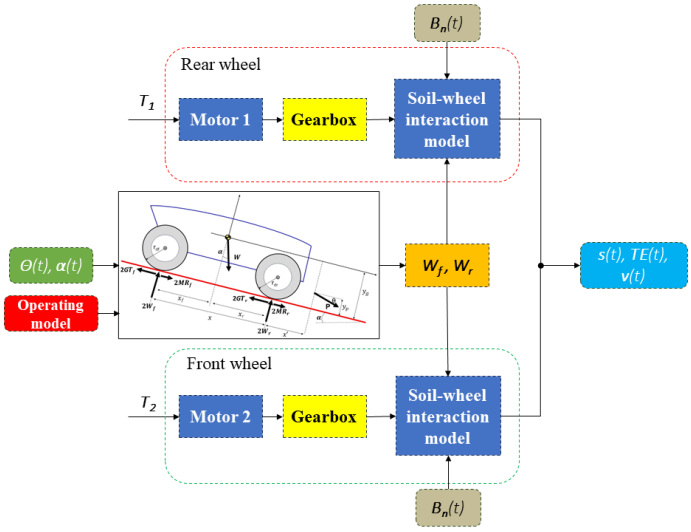

Figure 2. Overall framework of the dynamic model of an electric tractor with

3. RESULTS AND DISCUSSION.

3.1 Generation of power distribution maps.

Each wheel has its traction efficiency based on the traction capacity it possesses at a given moment, but it is also important to assess the overall traction efficiency, i.e., the combined efficiency resulting from the entire vehicle. Figure 3(a) depicts the front tire traction efficiency in relation to the percentage of power applied to it and the ground slope angle, ranging from -10º to 10º. It can be observed that the maximum power that can be applied to the front tire on an uphill of 10º does not exceed 25% of the total vehicle power, beyond this power level, there is no traction capacity due to the decrease in the front dynamic weight, $\boldsymbol{W_f}$, as the vehicle rises. Conversely, in Figure 3(b), the power applied to the rear tire can reach up to 70%, as its traction capacity increases due to the increase in $\boldsymbol{W_r}$ as the vehicle goes uphill. Figure 4(c) illustrates the overall vehicle traction efficiency, where it can be observed that during uphill travel, the power at the rear wheel must be increased to ensure traction capacity; otherwise, there will be no traction, as indicated in the white region of the graphic. These power distribution maps can be used to identify the optimal distribution constant $\boldsymbol{a}$ for each case, in which it will deliver the maximum traction efficiency.

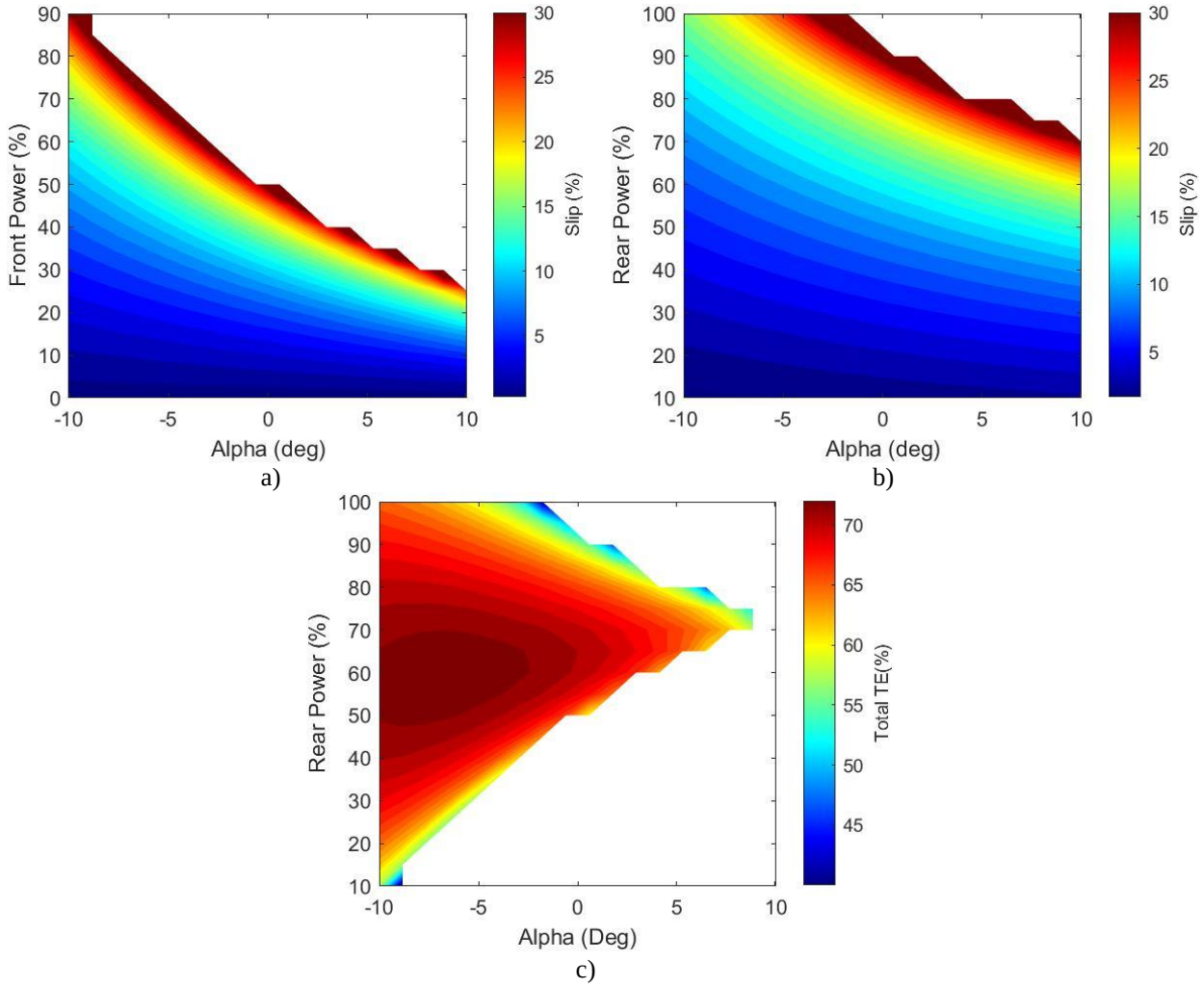

Figure 3. Maps of power distribution by wheel.

3.2 Dynamic operation simulation

Implementing the dynamic model in Matlab Simulink®, Figure 4 presents the results obtained during 120 seconds of operation, as previously described. Figure 4(a) illustrates the behavior of wheel slip for both the front wheels (blue) and the rear wheels (red) of the tractor over the operational cycle. An increase in slip is observed as soon as the tractor is set in motion, followed by stabilization after the speed becomes constant. Slip increases again when the working operation begins, as the drag implement penetrates the soil. As the ground slope begins after traveling 50 meters, with an angle $\boldsymbol{\alpha}$ of 10°, the front wheel starts to lose grip with the ground due to the weight distribution favoring the rear wheel of the

tractor, leading to another increase in front wheel slip, which occurs around 18 seconds. The working operation ends at 45 seconds; however, the terrain slope continues until it reaches 150 meters, which in this simulation occurred at approximately 60 seconds. The working operation restarts, but now on flat terrain, i.e., $\boldsymbol{\alpha} = 0°$. Under this condition, there is less slip in the front wheel and more slip in the rear wheel compared to the previous working operation. This behavior occurs because the dynamic weight on the front wheel decreased on flat terrain, resulting in a slight loss of traction capacity. Figure 4(b) presents the forward speed of the tractor, where the behavior influenced by the slip of the front and rear wheels can be observed. The speed decreases both at the beginning of the working operation and due to the terrain slope, depending on speed control to keep it stable. This control is of great importance since some agricultural operations with drag implements require a constant speed throughout the working operation. Figure 4(c) shows the variation in traction efficiency throughout the operations. It is possible to observe a decrease in front wheel traction efficiency compared to the rear at the beginning of the working operation due to the presence of the drag force of the implement with a slope at the rear of the vehicle. Additionally, traction efficiency decreases during the terrain slope, resulting in a loss of traction capacity. In moments when there are no significant opposing forces that need to be overcome, traction efficiency is equal to zero. This occurs because the assessment of traction efficiency is not relevant when there are no opposing forces to be overcome, such as during maneuvering operations when the speed is constant.

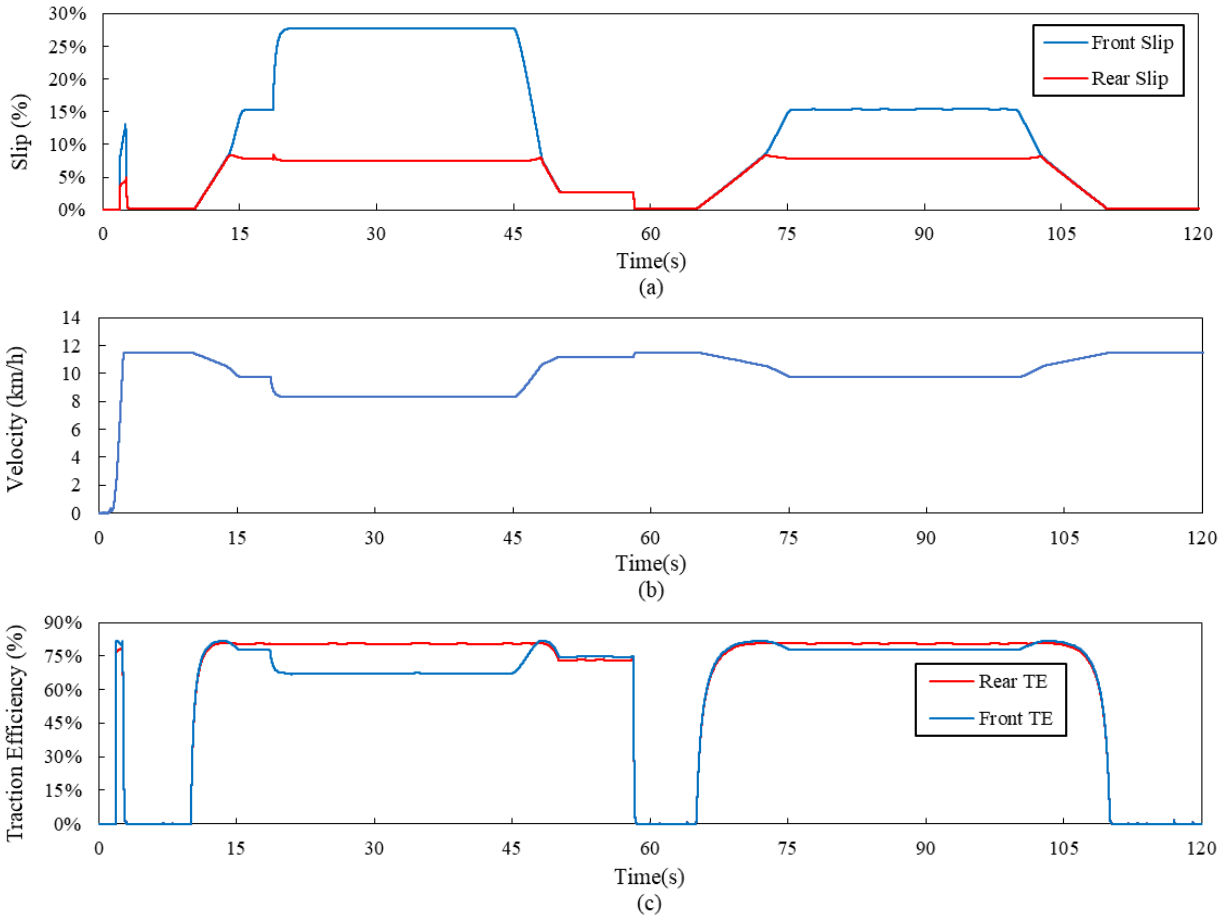

Figure 4. Overall framework of the dynamic model of an electric tractor with

4. ACKNOWLEDGEMENTS

We thank Professor Angel Garcia for all the knowledgements in simulation implementation, and Professor Tarcio Barros for all the knowledgements in electric motors, and Professor Daniel Albiero for all the knowledgements in traction phenomenon. This work was funded by FUNDEP under grant number 03-P-30156/2021.

5. CONCLUSIONS

Through simulation, divided into two phases - the maneuvering operation, where the electric tractor goes from rest to reach a certain speed by applying a torque ramp signal, and the working operation, where the drag implement comes into action - it was possible to observe the changes in traction parameters and the dynamic behavior in response to system

disturbances. These changes had a significant influence on traction efficiency and operational speed, a parameter that should remain constant during work. Through the control strategy that distributes torque according to the dynamic weight acting on each wheel, the generation of a power distribution map helps to determine percentage values of this distribution, aiming for maximum traction efficiency according to traction conditions at that moment. The dynamic modeling of the electric tractor, its operation, and the torque distribution map can be applied to the development of a future traction control system for electric tractors with independent motors on each wheel.

6. REFERENCES

Brixius, W. W. (1987). Traction prediction equations for bias-ply tires. *ASAE Paper No. 871622*. St. Joseph, Mich.: ASAE

Chen, T., Chen, L., Xu, X., Cai, Y., & Sun, X. (2019). Simultaneous path following and lateral stability control of 4WD-4WS autonomous electric vehicles with actuator saturation. *Advances in Engineering Software*, *128*, 46–54. https://doi.org/10.1016/j.advengsoft.2018.07.004

Cong, G., Biao, J., & Xin, Z. (2018). Research on Torque Control Strategy for Electric Vehicle with In-wheel Motor. *IFAC-PapersOnLine*, *51*(31), 71–74. https://doi.org/10.1016/j.ifacol.2018.10.014

Grisso, R., Perumpral, J., & Zoz, F. (2006). An empirical model for tractive performance of rubber-tracks in agricultural soils. *Journal of Terramechanics*, *43*(2), 225–236. https://doi.org/10.1016/j.jterra.2005.12.002

Macmillan, R. H. (2010). The Mechanics of Tractor-Implement Performance Theory and Worked Examples. http://www.eprints.unimelb.edu.au

Osinenko, P., & Streif, S. (2017). Optimal traction control for heavy-duty vehicles. *Control Engineering Practice*, *69*, 99–111. https://doi.org/10.1016/j.conengprac.2017.09.010

Rajamani, R. (2012). *Vehicle Dynamics and Control*. Springer US. https://doi.org/10.1007/978-1-4614-1433-9

Wang, J., Gao, S., Wang, K., Wang, Y., & Wang, Q. (2021). Wheel torque distribution optimization of four-wheel independent-drive electric vehicle for energy efficient driving. *Control Engineering Practice*, *110*. https://doi.org/10.1016/j.conengprac.2021.104779

Wang, S., Wu, X., Zhao, X., Wang, S., Xie, B., Song, Z., & Wang, D. (2023). Co-optimization energy management strategy for a novel dual-motor drive system of electric tractor considering efficiency and stability. *Energy*, *281*, 128074. https://doi.org/10.1016/j.energy.2023.128074

Xie, B., Wang, S., Wu, X., Wen, C., Zhang, S., & Zhao, X. (2022). Design and hardware-in-the-loop test of a coupled drive system for electric tractor. *Biosystems Engineering*, *216*, 165–185. https://doi.org/10.1016/j.biosystemseng.2022.02.014

7. RESPONSIBILITY NOTICE

The authors are the only responsible for the printed material included in this paper.